IEEE Transactions on Industry Applications, Vol. 40, 2004

Design of Fast and Robust Current Regulators for High Power Drives based on Complex State Variables

J. Holtz†, *Fellow, IEEE,* J. Quan‡, G. Schmitt†, J. Pontt O.*, J. Rodriguez P.*, P. Newman* and H. Miranda*

† Machines and Drives Group
University of Wuppertal
42097 Wuppertal – Germany

‡ Rockwell Automation AG
Luzern – Switzerland

* Departamento de Electronica
Universidad Federico Santa María
Valparaíso – Chile

Abstract – **High-power PWM inverters for medium voltage applications operate at switching frequencies below 1 kHz to keep the dynamic losses of the power devices at permitted level. Also the sampling rate of the digital signal processing system is then low, which introduces considerable signal delays. These have adverse effects on the dynamics of the current control system and introduce undesired cross-coupling between the current components i_d and i_q.**

To overcome this problem, complex state variables are used to derive more accurate models of the machine and the inverter. From these, a novel current controller structure employing single-complex zeroes is synthesized.

Experimental results demonstrate that high dynamic performance and zero cross-coupling is achieved even at very low switching frequency.

Keywords: Induction motor, current control, medium voltage inverters, low switching frequency, complex state variables, root locus techniques

I. Introduction

The dynamic analysis of induction motors is traditionally based on state equations, with the *d*- and *q*-axis components of the stator currents and the rotor flux linkage as state variables [1]. The electromagnetic subsystem of the machine is usually modeled as a 4th-order dynamic system in terms of scalar state variables. Although the root locus plot is easily obtained in this approach, it appeared difficult so far to utilize this powerful tool of dynamic system analysis for the design of current controllers in ac drives. Root locus techniques are indeed being considered being hardly useful for this purpose. It is frequently commented in the literature that the obstacle is the dynamic complexity of the induction motor [2]. The design of the current control system of an induction motor drive is therefore commonly based on an approximation: the intercoupled 4th-order system is replaced by two independent 1st-order systems, one for each current component.

This paper uses space vector state variables to model the induction motor. A rigorous approach enables a root locus based design of the current control system and facilitates the definition of new control structures. A comparison is made between conventional and the new complex current controllers. The improvements are documented by experiments.

II. Machine Models

A. Scalar versus complex machine model

The complex state variable approach for the dynamic analysis of ac machines was presented in two earlier publications, [3] and [4]. It was demonstrated that the complex eigenvalues of the system represent dynamically independent components of transient energy. The definition of transient energy of an ac machine is given in [4]. Not considering the mechanical inertia, the transient energy of an induction motor is stored in its magnetic fields. There are only two dynamically independent entities of magnetic energy. Physically, these relate to the main flux and the leakage fluxes, respectively. Given the predominantly sinusoidal distribution in space of the magnetic fields, each entity is characterized by an amount of energy and its spatial orientation, being represented by the amplitude of a sinusoidal flux density distribution and its phase angle. It appears stringent, therefore, to use space vectors as the state variables to represent the total transient energy. The electromagnetic subsystem of an induction machine is thus modeled as a 2nd-order system in terms of two complex state variables [3].

Subsequent linear transformations permit representing the main flux and the leakage fluxes by the respective space vectors of the stator flux linkage and the rotor flux linkage, or the stator current and the rotor flux linkage, or other appropriate space vectors.

Modelling of ac machines in terms of complex space vectors has been previously reported in the literature. Many authors consider the complex vector representation by a 2nd-order model equivalent to the scalar representation of a 4th-order model, arguing that both models give the same results [5]. It is indeed a very straightforward mathematical operation that converts a 2nd-order complex vector model of the machine to the scalar 4th-order model, and vice versa. Although apparently mathematically correct, the operation changes the physical significance of the system eigenvalues. This is a strong argument against the equivalence of the two models. It is in fact only the complex state variable model that permits a physical interpretation of transient machine behavior, as its two eigenvalues refer directly to the two entities of transient energy inside the machine [4]. Against this, the 4th-order scalar model must be considered an approximation. It replaces the spatially distributed magnetic energy by the energy of concentrated inductors. These form the elements of coupled, lumped-parameter circuits [1]. The response to a transient excitation is *time-dependent oscillations*, while the

original dynamic process is commanded by the interaction between distributed magnetic energies which results in their *spatial displacement*.

To understand the difference between the scalar model and the complex state-variable model, a more rigorous definition is needed of a space vector than that originally given by Kovács and Rácz [6]. Neglecting space harmonics, the flux density distribution in the airgap of an ac machine is sinusoidal. According to the original concept, such sinusoidal distribution is uniquely described by a space vector. It was found convenient to use the flux linkages of the distributed machine windings for machine analysis instead of the distributed flux densities, which is equivalent. Current and voltage space vectors were subsequently defined with reference to the respective phase currents and phase voltages, thus introducing scalar circuit parameters. The two-axis-transformation [l] eliminates the zero-sequence component of a three phase system, representing the three phase currents by their two orthogonal *d*- and *q*-components. However, two scalar components cannot be considered an equivalent to a complex space vector. The use of scalar components as state variables entails a division in two portions of the continuous spatial distributions that represent the transient state of the system only as a whole.

Following from this, a space vector is not just a complex variable which could be formally separated in two independent orthogonal components; instead, it is an entity of its own class, which describes a continuous, sinusoidal distribution in space. It is the total energy assigned to such distribution that represents the transient system state; this energy is inherently indivisible.

To elaborate on this, a current shall be considered that flows in one distributed phase winding, while the other phase windings are deenergized. Since space harmonics are neglected, the winding conductors are necessarily arranged in a spatially sinusoidal density pattern. Hence the phase current under consideration generates a sinusoidal current density distribution, thus defining a current space vector of determined magnitude and phase angle. The phase angle is fixed in space as the winding axis is fixed. The resulting magnetic field represents the associated energy.

Expanding on this, there is no basic difference when all phase currents in a polyphase winding are nonzero. The current density distributions of the individual phase currents superimpose to form a resulting distribution, which is again spatially sinusoidal; it is described by the space vector of the polyphase current system. The resulting magnetic field establishes a spatial distribution of magnetic energy. The magnitude and spatial orientation of this distribution can assume any values, depending on the respective magnitudes of the phase currents.

Also voltage vectors are representatives of sinusoidal distributions. The resistive voltage drop in a distributed winding arrangement of sinusoidal winding density exhibits necessarily a sinusoidal variation in space. The same is true for the induced voltage, which is also distributed in space; it is proportional to the local winding density.

B. The complex state variable model

The spatial information is accurately conserved when the complex state variable approach is followed. The state equations of the electromagnetic subsystem of an induction motor are written as

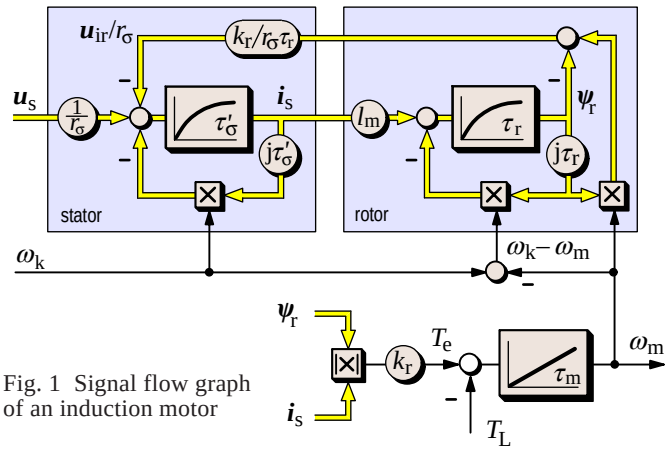

Fig. 1 Signal flow graph of an induction motor

$$\tau'_\sigma \frac{d\boldsymbol{i}_s}{d\tau} + \boldsymbol{i}_s = -\mathrm{j}\omega_k \tau'_\sigma \boldsymbol{i}_s + \frac{k_r}{\tau_r r_\sigma}(1 - \mathrm{j}\tau_r\omega_m)\boldsymbol{\psi}_r + \frac{1}{r_\sigma}\boldsymbol{u}_s \qquad (1a)$$

$$\tau_r \frac{d\boldsymbol{\psi}_r}{d\tau} + \boldsymbol{\psi}_r = -\mathrm{j}(\omega_k - \omega_m)\tau_r \boldsymbol{\psi}_r + l_m \boldsymbol{i}_s \qquad (1b)$$

where the normalized space vectors $\boldsymbol{i}_s$ of the stator current and $\boldsymbol{\psi}_r$ of the rotor flux linkage are the two state variables of a 2nd-order system. ω_m is the mechanical angular velocity of the motor shaft. The parameters in (1) are $\tau'_\sigma = \sigma l_s/r_\sigma$, $r_\sigma = r_s + k_r^2\, r_r$, and $k_r = l_m/l_r$, where $\sigma = 1 - l_m^2/l_s l_r$ is the total leakage coefficient. The angular velocity of the reference frame is denoted by a general value ω_k. It is assumed that the mechanical time constant of the motor is much larger than the transient time constants of the electromagnetic subsystem, and hence ω_m = const. is a valid approximation. Note that time is also normalized: $\tau = \omega_{sR} t$, where ω_{sR} is the nominal stator frequency.

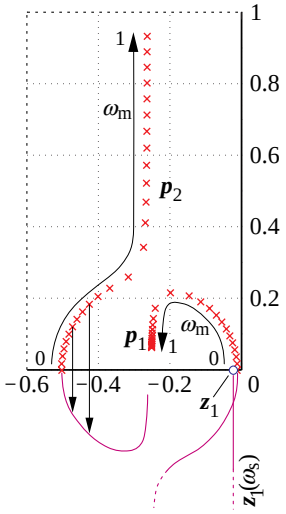

Fig. 2 Root loci of the induction motor, ω_m = 0 … 1 par, stationary coordinates; lower curve; root loci transformed to synchronuos coordinates

A visual representation of (1) is the signal flow graph Fig. 1, where $\boldsymbol{u}_{ir}$ is the rotor induced voltage in the stator winding. The significance of complex signal flow graphs is detailed in [3].

When designing the current control system, $\boldsymbol{u}_s$ is considered as the input, and $\boldsymbol{i}_s$ is the output variable of the motor. The transfer function of the induction motor is derived from (1) choosing synchronous coordinates, $\omega_k = \omega_s$,

$$\boldsymbol{F}_m(s) = \frac{\boldsymbol{I}_s(s)}{\boldsymbol{U}_s(s)} = \frac{1}{r_\sigma} \cdot \qquad (2)$$

$$\frac{(\tau_r s + 1 + \mathrm{j}\omega_r \tau_r)}{(\tau'_\sigma s + 1 + \mathrm{j}\omega_s \tau'_\sigma)(\tau_r s + 1 + \mathrm{j}(\omega_s - \omega_m)\tau_r) - k_1(1 - \mathrm{j}\omega_m \tau_r)}$$

where $\boldsymbol{U}_s(s) = L\{\boldsymbol{u}_s(t)\}$ and $\boldsymbol{I}_s(s) = L\{\boldsymbol{i}_s(t)\}$ are the respective Laplace transforms, $\omega_r = \omega_s - \omega_m$ is the electrical rotor frequency, and $k_1 = k_r\, l_m/(r_\sigma \tau_r)$ is a constant machine parameter.

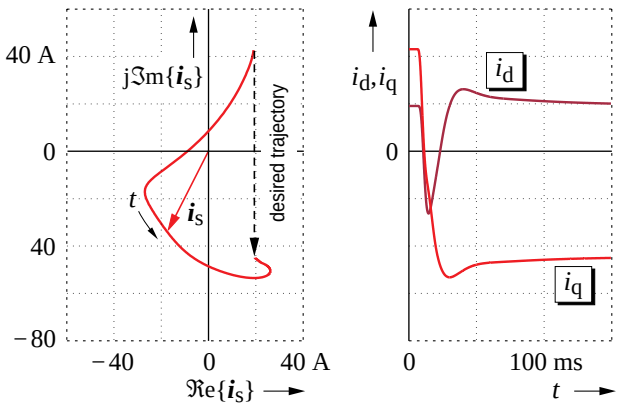

Fig. 3 Cross-coupling between the current components in a PI-controlled induction motor drive; operation at rated speed and 500 Hz switching frequency (simulation)

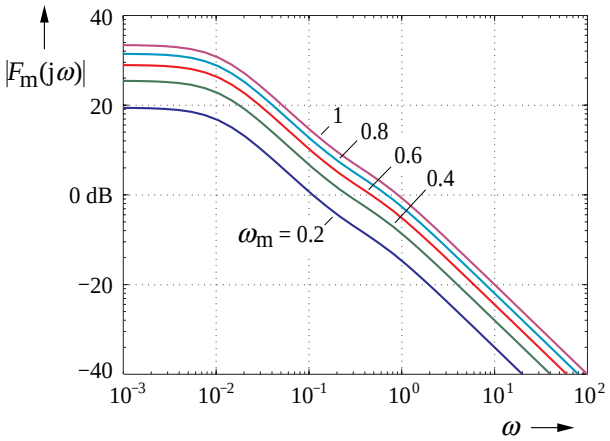

Fig. 4 Cross frequency response of the induction motor; ω_m = par.

$\boldsymbol{F}_m(s)$ in boldface notation underlines the complex nature of this transfer function. This property is owed to the existence of complex coefficients.

As the dynamics of the load are not modelled, $\omega_r = 0$ is assumed throughout. The solution of the characteristic equation of (2) defines the locations in the complex plane of the two single-complex poles $\boldsymbol{p}_1(\omega)$ and $\boldsymbol{p}_2(\omega)$, and the numerator contributes a zero $\boldsymbol{z}_1$. These are plotted in Fig. 2 in stationary coordinates, $\omega_k = 0$, as functions of the angular velocity ω_m of the rotor. The zeroes of the transfer function (2) are marked by circles. A physical interpretation given in [4] assigns a particular distribution in space of transient magnetic energy to each pole. The rate of energy decay is determined by the respective real part. The imaginary part defines the direction and angular velocity at which the magnetic energy displaces during a transient process with respect to the chosen reference frame. This definition of the angular velocity is unique as eigenvalues of complex state variables have only one imaginary part. Contrasting to this, the eigenvalues of the scalar machine model result as conjugate complex pairs that do not define a particular direction of rotation. This is one of the deficiencies of the scalar model.

A transformation of the root loci to synchronous coordinates can be done by simply substracting the respective ω_s-values from the imaginary component of all roots as indicated in the lower portion of Fig. 2, and exemplified by arrows. The resulting curves are the root loci in synchronous coordinates, $\omega_k = \omega_s$. The same result is obtained by letting $\omega_k = \omega_s$ in (1) and subsequently computing the system eigenvalues.

The graphs demonstrate that the transient magnetic fields, characterized by the poles $\boldsymbol{p}_1(\omega)$ and $\boldsymbol{p}_2(\omega)$, rotate in a positive direction in the stationary reference frame, and in a negative direction in synchronous coordinates, [4]. The constant zero $\boldsymbol{z}_1 = -1/\tau_r$ in stator coordinates gets expanded to the trajectory $\boldsymbol{z}_1(\omega_s) = -1/\tau_r - j\omega_s$ when the system is viewed in synchronous coordinates.

C. Complex transfer functions

Having introduced complex state variables to analyze the dynamics of the induction motor and its control, the pertaining transfer functions have complex coefficients and hence are also complex in general. This can be easily seen from the transfer function (2) of the induction motor.

The complex transfer function of the closed loop current control system can be written as

$$\boldsymbol{F}_c(s) = \frac{\boldsymbol{I}_s(s)}{\boldsymbol{I}_s^*(s)} = Re\{\boldsymbol{F}_c(s)\} + jIm\{\boldsymbol{F}_c(s)\}, \qquad (3)$$

where $\boldsymbol{I}_s(s)$ and $\boldsymbol{I}_s^*(s)$ are the respective Laplace transforms of $\boldsymbol{i}_s(t)$ and $\boldsymbol{i}_s^*(t)$. The transfer function (3) shall be used to assess the dynamic performance of the current control system.

In a transient process, the adjustment of the current space vector to a change of its reference value is retarded by various delays. These are caused by the eigenbehavior of the machine, and by the delay of the inverter and the time-discrete sampling of the digital control. It is important that the trajectory of the current space vector gets adjusted such that both the commanded torque and magnetic excitation of the machine are established at minimum time delay. Contra-productive to this aim is the complex nature of the transfer function (3). It causes the adverse effect that the output vector of the system moves in a different spatial direction than the exciting input vector. As an example, Fig. 3 shows how the current control can react on a commanded change of only the imaginary current component i_q. While i_d is expected to maintain its commanded value, it gets heavily disturbed; it temporarily even reverses its polarity. The effect is amplified by a low value of switching frequency which is 500 Hz in this example.

A figure of merit to evaluate such undesired cross-coupling between the current components is developed next.

D. Cross frequency response

It is easily seen from (3) that the cross-coupling is formally introduced by the complex factor j. In general, it is the imaginary component $Im\{\boldsymbol{F}(s)\}$ of a complex transfer function that determines the amount of cross-coupling of a dynamic system $\boldsymbol{F}(s)$. To obtain the percentage of cross-coupling, $Im\{\boldsymbol{F}(s)\}$ shall be referred to the term $Re\{\boldsymbol{F}(s)\}$ that defines the direct throughput of the input signal. Of particular interest is the frequency response, $s = j\omega$, which leads to the definition of the normalized frequency response of cross-coupling

$$F_{xy}(j\omega) = \frac{Im\{\boldsymbol{F}_c(j\omega)\}}{Re\{\boldsymbol{F}_c(j\omega)\}} \qquad (4)$$

as a figure of merit to express the amount of cross-coupling.

Applying (4) to the transfer function (2) yields the cross frequency response of an induction motor. It is displayed in Fig. 4 for different mechanical angular rotor velocities ω_m.

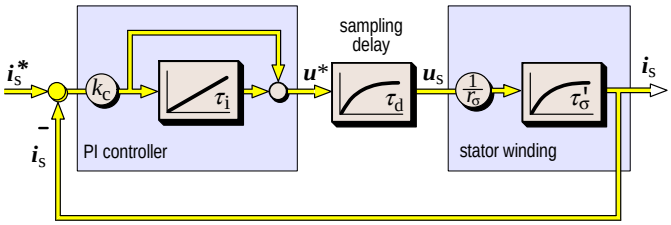

Fig. 5 Pl current control system; simplified machine model

These characteristics can be explained by examining the root loci of the motor, Fig. 2. A particular situation is $\omega_m = 0$, where both roots are real-valued since $\omega_s = \omega_m = 0$. Since also the zero of (2) is a real-valued constant, the transfer function has no imaginary component at $\omega_m = 0$. This indicates that no cross-coupling exists. Such situation does not reflect in Fig. 4 since zero values cannot be displayed in a logarithmic scale. As the velocity ω_m of rotation increases, both roots move into the 3rd quadrant of the complex plane; their imaginary parts increase in magnitude. This lets the imaginary component of the cross frequency response (2) increase, and the magnitude of the cross frequency response (4), at given frequency ω of excitation, rises in proportion to ω_m.

The variation with frequency of these curves is explained looking at the poles $\boldsymbol{p}_i$ and zeros $\boldsymbol{z}_i$ of (2), the locations of which are shown in Fig. 2. The magnitude of $F_{xy}(j\omega)^{IM}$ is constant at low frequencies and changes to a –20-dB/decade decline at $\omega > -|\boldsymbol{p}_1|$. The slope increases slightly around $\omega = -|\boldsymbol{z}_1|$, while readjusting to –20 dB/decade at higher frequency. This is because $\boldsymbol{p}_2 \approx \boldsymbol{z}_1$which almost cancels their effect. The cross frequency response is then dominated by $\boldsymbol{p}_1$.

It is an adverse property of this system that the cross-coupling gain is high over most of the frequency range, peaking up to about 34 dB at low excitation frequency and rated speed, $\omega_m = 1$.

The problem persists, in principle, when the machine is operated at closed-loop current control. Existing current controllers exhibit real-valued roots and zeroes and thus do not satisfactorily manipulate the single-complex eigenvalues of the machine and the inverter. It is only by virtue of the zero steady-state error property of PI controllers that the existing cross-coupling gets compensated when the transients have died out. It depends on the bandwidth of the current control system how fast the transient error is eliminated. The dynamic error is tolerable when the control bandwidth is much higher than the eigenfrequencies of the machine. The critical margin however narrows

- when the control bandwidth reduces, as in high-power inverters that operate at low switching frequency, or
- when the machine eigenfrequencies increase, which happens at higher speed in the field weakening range.

Both conditions tend to increase the undesired cross-coupling.

State-of-the-art current control techniques [7] cannot handle this problem in a satisfying manner. Before developing an improved strategy, the existing current control methods will be evaluated against the performance requirements.

III. Methods of Current Control

A. Hysteresis current control

A hysteresis controller instantaneously applies high amplitude voltages to the machine terminals whenever a preset error margin in space in exceeded, thus forcing the stator current vector to return close to the neighborhood of its reference vector. The high stator voltages completely override the machine dynamics which makes hysteresis current control an extremely robust approach. Cross-coupling is also eliminated. The drawback of this method is the high harmonic content of the machine currents which renders hysteresis control inapplicable at medium and low switching frequency [8]. Hence it is mostly preferred to use linear current controllers and to generate the switching sequence by a pulsewidth modulator.

B. PI current controller with real-valued time constant

The most common implementation uses Pl current controllers in synchronous coordinates for the two current components in field coordinates, i_d and i_q. The complex notation merges the two controllers into a single controller having the transfer function

$$\boldsymbol{F}_r(s) = k_o \frac{(\tau_i s + 1)}{\tau_i s}\ , \tag{5}$$

where the controller time constants τ_i are real-valued, $k_o = r_\sigma g_o$ is a coefficient and g_o is the open loop gain. The complex signal flow graph of the PI controller is shown in the left of Fig. 5.

A first order delay τ_d models the PWM inverter and the time delays that result from processing the signals as sampled data. The sampling delay is commonly represented by

$$\boldsymbol{F}_d(s) = \frac{1}{(\tau_d s + 1)} \tag{6}$$

where $\tau_d = 1.5/2f_s$ is the delay time, $2f_s$ is the sampling frequency of the microprocessor, and f_s is the switching frequency of the inverter.

Neglecting the inverter and sampling delay [5], [9] is only permitted if the switching frequency is much higher than the characteristic eigenfrequencies of the motor.

The design of the controller is normally based on a simplified open loop transfer function. It is obtained from Fig. 5 with reference to (5) and (6)

$$\boldsymbol{F}_o(s) = g_o \frac{(\tau_i s + 1)}{\tau_i s} \frac{1}{(\tau_d s + 1)} \frac{1}{(\tau_\sigma' s + 1)} \tag{7}$$

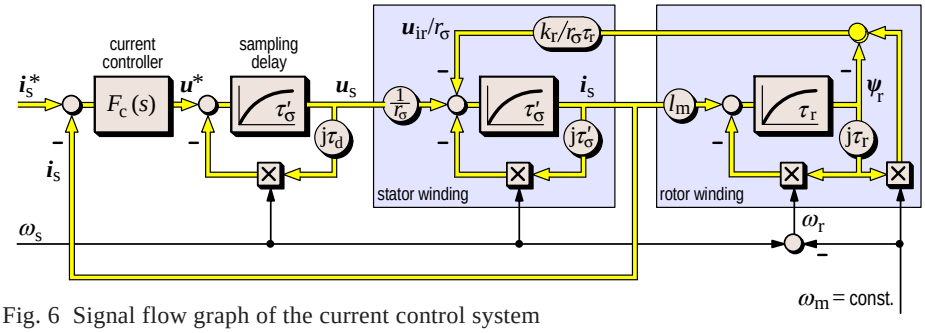

Fig. 6 Signal flow graph of the current control system

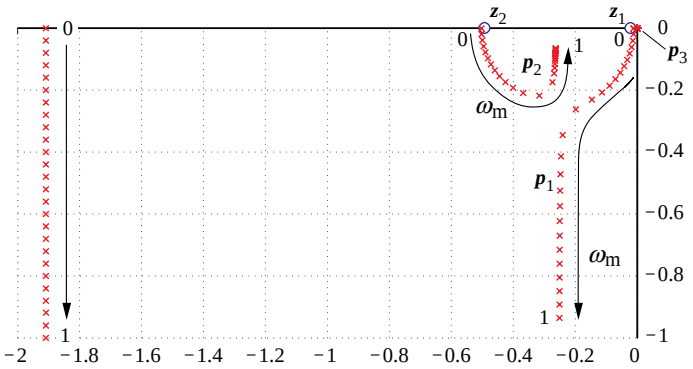

Fig. 7 Root loci of the open loop system, PI control, synchronous coordinates; par: $\omega_m = 0 \ldots 1$

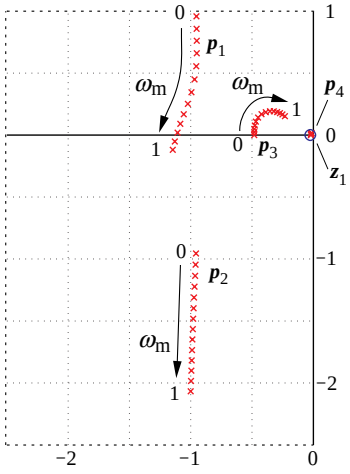

Fig. 8 Root loci of the closed loop system, PI control, synchronous coordinates; f_s = 500 Hz, $\omega_m = 0 \ldots 1$ parameter

The controller time constant τ_i in (7) is determined with reference to the per-phase equivalent circuit of the machine, in which the stator current dynamics are dominated by the transient time constant τ_σ'. Such approximation neglects the imaginary parts of the coefficients in (2). Accordingly, all cross-coupling links in Fig. 1 disappear in Fig. 5. The PI controllers for the respective current components i_d and i_q then operate independently from each other. Their time constants are selected as $\tau_i = \tau_\sigma'$, which makes the sampling frequency $1/\tau_d$ determine the controller bandwidth. The open loop gain g_o is set for a given damping D of the closed loop system. Choosing $D = 1/2\sqrt{2}$ yields $g_o = \tau_\sigma'/2\tau_d$.

The performance of the simplified system is analyzed using the accurate machine model Fig. 1. Synchronous coordinates are selected, $\omega_k = \omega_s$. The resulting signal flow graph of the current control system is shown in Fig. 6.

The delays introduced by the PWM inverter and the time-discrete sampling are approximated by a first-order system

$$\tau_d \frac{d\boldsymbol{u}_s^{(S)}}{d\tau} + \boldsymbol{u}_s^{(S)} = \boldsymbol{u}^{*(S)}, \qquad (8)$$

where $\boldsymbol{u}^*$ is the reference voltage vector generated by the current controller. The variables are marked by the superscript $^{(S)}$ as being referred to in stationary coordinates.

Equation (8) is multiplied by the unity vector rotator $exp(-j\omega_s\tau)$ to effect a transformation to synchronous coordinates

$$\tau_d \frac{d\boldsymbol{u}_s}{d\tau} + (1 + j\omega_s\tau_d)\boldsymbol{u}_s = \boldsymbol{u}^*. \qquad (9)$$

Space vectors referred to in synchronous coordinates are not specifically marked in the following.

A transformation of (9) to the frequency domain yields the

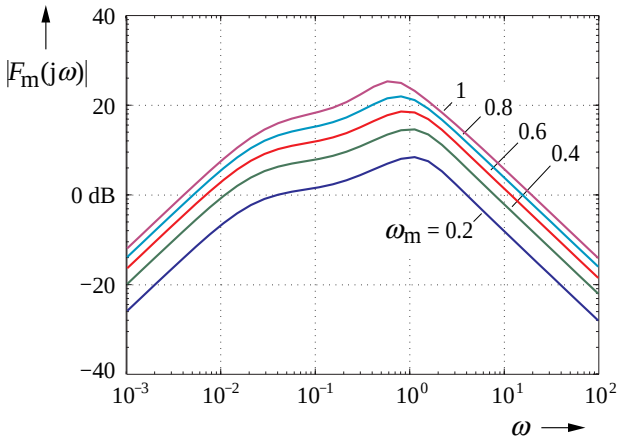

Fig. 9 Cross frequency response of the closed loop system, PI controller

transfer function of the inverter and sampling delay

$$\boldsymbol{F}_d(s) = \frac{\boldsymbol{U}_s(s)}{\boldsymbol{U}^*(s)} = \frac{1}{(\tau_d s + 1 + j\omega_s\tau_d)} \qquad (10)$$

where $\boldsymbol{U}_s(s) = L\{\boldsymbol{u}_s(t)\}$ and $\boldsymbol{U}_s^*(s) = L\{\boldsymbol{u}_s^*(t)\}$ are the respective Laplace transforms of the input and the output signal. Note that $\boldsymbol{F}_d(s)$ is a transfer function having complex coefficients.

The open loop transfer function of the current control system is obtained from (2) and (10),

$$\boldsymbol{F}_o(s) = \boldsymbol{F}_r(s) \cdot \frac{1}{(\tau_d s + 1 + j\omega_s\tau_d)} \qquad (11)$$

$$\cdot \frac{(\tau_r s + 1 + j\omega_r\tau_r)/r_\sigma}{\left(\tau_\sigma'\tau_r s^2 + (\tau_\sigma' + \tau_r)s + (1 - k_1)\right) + j[\omega_s\tau_\sigma'(\tau_r s + 1) + k_1\omega_m\tau_r]}$$

where $\boldsymbol{F}_r(s)$ is the transfer function (5) of the current controller. $\boldsymbol{F}_o(s)$ is of 4th order in terms of complex state variables. With a view towards high power applications, the switching frequency is chosen as f_s = 500 Hz which corresponds to a normalized time constant $\tau_d = 0.35$. The time constant of the current controller $\boldsymbol{F}_r(s)$ is again chosen as $\tau_i = \tau'_\sigma$, which positions the zero $\boldsymbol{z}_2$ in Fig. 7. This plot shows the locations of the 4 poles and 2 zeros in the base speed range. Only at zero speed gets the machine pole $\boldsymbol{p}_2$ canceled by the numerator term of the controller (zero $\boldsymbol{z}_2$), although not exactly.

Fig. 8 shows the root loci of the closed loop system. As per

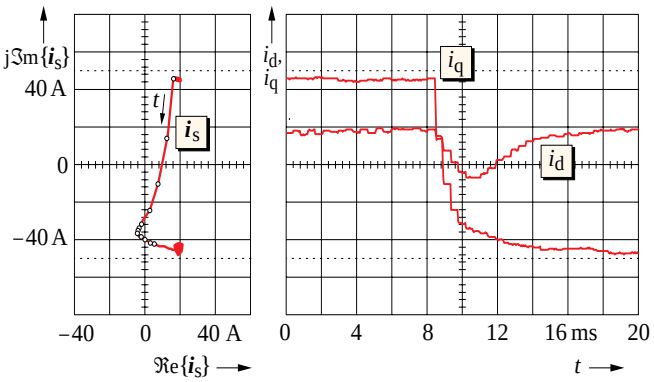

Fig. 10 Recorded step response of the current control system, PI controller, f_s = 1100 Hz

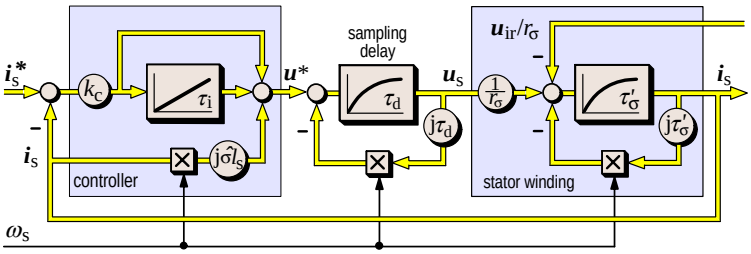

Fig. 11 Pl current control with feedforward compensation

the design, the roots $\boldsymbol{p}_1$ and $\boldsymbol{p}_2$ are critically damped at zero speed, being located symmetrically at ±45° with respect to the negative real axis. The situation is much different at nonzero speed. The complex nature of the state variables is then reflected in asymmetric pole locations with respect to the real axis. Pole positions having unbalanced imaginary parts indicate that cross-coupling between the current components exists. The cross frequency response function (4) then becomes nonzero, which makes the current space vector deviate from its commanded trajectory as in Fig. 3. A balance between the imaginary parts of the single-complex poles in Fig. 8 exists only at $\omega_m = 0$ where $\boldsymbol{p}_1 = \boldsymbol{p}_2^*$ form what looks like a conjugate complex pair, and $\boldsymbol{p}_3$ and $\boldsymbol{p}_4$ are real-valued.

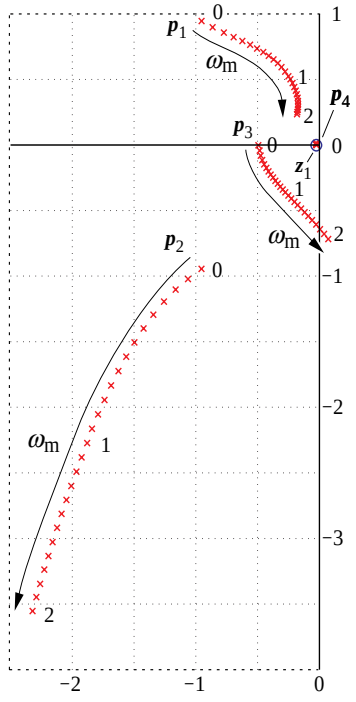

Fig. 12 Root loci using Pl control with feedforward compensation, synchronous coordinates; f_s = 500 Hz, ω_m = 0 … 2 parameter

The particular situation $\boldsymbol{p}_1 = \boldsymbol{p}_2^*$ is different from what is normally known as a conjugate complex pair $\lambda_1 = a + jb = \lambda_2^* = (a - jb)^*$, being roots of a characteristic equation with real coefficients. Such roots λ_1, λ_2 are scalars. Against this, each of the roots $\boldsymbol{p}_1$, $\boldsymbol{p}_2$ is single-complex. Only at $\omega_m = 0$ do these roots happen to have equal imaginary parts of opposed sign for the system under consideration. They do not form a pair in the sense that λ_1, λ_2 do.

The cross-coupling frequency response $|F_{xy}(j\omega)|$ Fig. 9 shows reduced gain at frequencies below 5 Hz ($10^0 \rightarrow \omega_{sR}$ = 314 $^{s-1}$) as compared with the behavior of the uncontrolled machine, Fig. 4.

Experimental results were obtained from a 30-kW induction motor drive operating at the relatively high switching frequency of 1100 Hz. The machine was run in a current controlled mode at nominal speed and nominal excitation. The load torque was first set to its nominal positive value, and the i_q-command was then reversed to its nominal negative value. Fig. 10 shows how the stator current trajectory deviates from its commanded track as i_d temporarily also reverses. It takes about 10 ms until the undesired cross-coupling is compensated.

The controlling microprocessor was programmed to acquire the respective current values in field coordinates. The data were passed through D/A converters to be visualized on an oscilloscope. It is for this reason that time-discrete values are seen in Fig. 10 which occurs at a sampling rate of $2f_s$ = 2.2 kHz.

C. PI current controller with feedforward compensation

An improved model of the induction motor reflects the fact, that cross-coupling exists in the stator winding when synchronous coordinates are used, Fig. 11. A feedforward compensation signal $j\omega_s\hat{\sigma}l_s\boldsymbol{i}_s$ is added to the PI controller. The voltage $j\omega_s\hat{\sigma}l_s\cdot\boldsymbol{i}_s$ is intended to cancel the internal, motion induced voltage $-j\omega_s\tau_\sigma'\cdot r_\sigma\boldsymbol{i}_s$ in the stator winding. Note that $\sigma l_s = r_\sigma\,\tau_\sigma'$. The method works well at high switching frequency where the inverter and sampling delay is negligible. The compensation signal is retarded at low switching frequency by a large inverter and sampling delay τ_d; the compensation is then erroneous and cross-coupling persists. Another source of uncompensated cross-coupling is the voltage $\boldsymbol{u}_{ir}$ that the rotor induces in the stator winding, Fig. 11.

The performance of feedforward compensation is studied by inserting the compensated PI controller of Fig. 11 into the current control system Fig. 6. The resulting closed loop transfer function is shown in (12) below. The root locus plot Fig. 12 was computed for 500 Hz switching frequency. There is still a clear tendency of the three single-complex roots to show unbalanced imaginary parts as the angular mechanical velocity ω_m increases. Moreover, the system gets unstable at higher speed. The reason is that the feedforward decoupling is counteracted by the phase shift of the inverter at higher frequencies. The performance is not improved as compared with that of the PI-controlled system, nor is the cross-coupling response at nominal speed Fig. 13 much better than that of Fig. 9.

The oscillograms taken experimentally at 1100 Hz switching

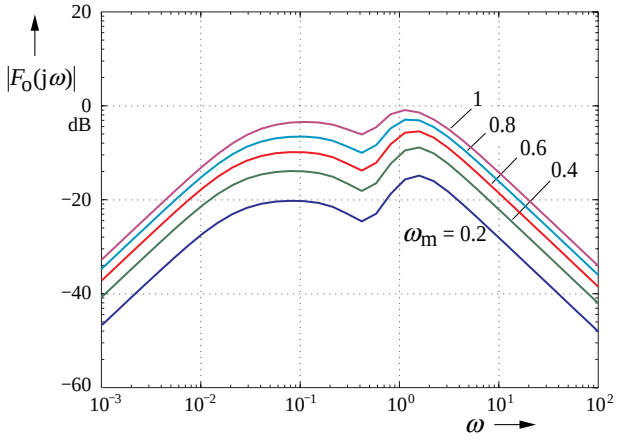

Fig. 13 Cross frequency response of the closed loop system, Pl controller with feedforward compensation

$$\boldsymbol{F}_c(s) = \frac{g_o\cdot(\tau_i s+1)(\tau_r s+1)}{\tau_i s((\tau_\sigma' s+1'+j\omega_s\tau_\sigma')(\tau_r s+1)-k_1(1-j\omega_m\tau)(\tau_d s+1+j\omega_s\tau_d)-j\omega_s\tau_\sigma'(\tau_r s+1))+g_o(\tau_i s+1)(\tau_r s+1)} \qquad (12)$$

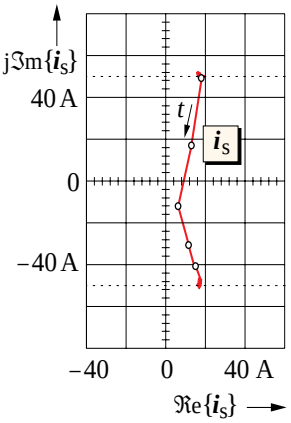

Fig. 14 Recorded step response of the current control system, PI control with feedforward compensation, synchronous coordinates; f_s = 1100 Hz

frequency confirm these results. The current trajectory in Fig. 14 still deviates from the desired path. An added problem is the inherent parameter sensitivity of feedforward control. A 20% error of the leakage inductance $\hat{\sigma l}_s$ leads to the much higher deviation shown in Fig. 15.

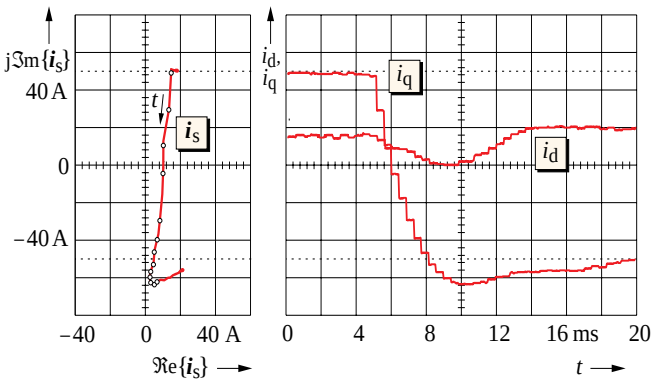

Fig. 15 Recorded step response as in Fig. 14, 20% parameter error

D. Current controller with single-complex poles

The foregoing analysis of established current control schemes has served to provide a better understanding of the dynamic properties of ac machines. This is owed to the use complex state variable models. The root loci of the resulting single-complex system eigenvalues have been introduced as a valuable tool in this respect.

This technique is now expanded to create a novel class of controllers. Such controller is constructed using single-complex poles so as to better correspond to the unique dynamic properties of ac machines.

The components of the current control system are modeled without approximation. Referring to the signal flow graph Fig. 6, an open loop transfer function is derived from (2) and (10), considering no-load, $\omega_r = 0$, and $k_1 = k_r\, l_m /(r_\sigma \tau_r)$

$$\boldsymbol{F}_o(s) = \boldsymbol{F}_r(s)\frac{1}{(\tau_d s + 1 + j\omega_s\tau_d)} \cdot \frac{(\tau_r s + 1)/r_\sigma}{(\tau_\sigma' s + 1 + j\omega_s\tau_\sigma')(\tau_r s + 1) - k_1(1 - j\omega_m\tau_r)} \tag{13}$$

where $\boldsymbol{F}_r(s)$ is the controller to be designed. Its transfer function is constructed such that the single-complex eigenvalues of the plant are displaced onto the real axis of the complex plane. The current controller

$$\boldsymbol{F}_r(s) = k_o \cdot \frac{(\tau_{i3} s + 1 + j\omega_s\tau_{i3})}{\tau_{i3} s + 1} \cdot \frac{(\tau_{i1} s + 1 + j\omega_s\tau_{i1})(\tau_{i2} s + 1) - k_1(1 - j\omega_m\tau_{i3})}{\tau_{i1} s(\tau_{i2} s + 1)} \tag{14}$$

meets this requirement. The choice of the time constants

$$\tau_{i1} = \tau_\sigma', \qquad \tau_{i2} = \tau_r, \qquad \tau_{i3} = \tau_d \tag{15}$$

is appropriate. $k_o = r_\sigma g_o$ is a coefficient and g_o is the open loop gain.

The visualization of (14) in the left of the signal flow graph Fig. 16 illustrates how the complex current controller mirrors the system roots into its poles. The original signal flow graph of the induction motor Fig. 1 appears in the right of Fig. 16 in a rearranged layout. This serves for a better understanding of the elements of the complex controller in the left. The structure in the lower right of the current controller box in Fig. 16 compensates the complex inverter and sampling delay τ_d. It generates the chain of zeroes shown in the left of Fig. 17 at $-1/\tau_d - j\omega_s$ as function of ω_s, thus replacing the chain of poles by a single pole at $-1/\tau_d$ on the real axis.

The portion in the center aims at compensating the eigenbehavior of the stator. Its contributions are a chain of zeroes at

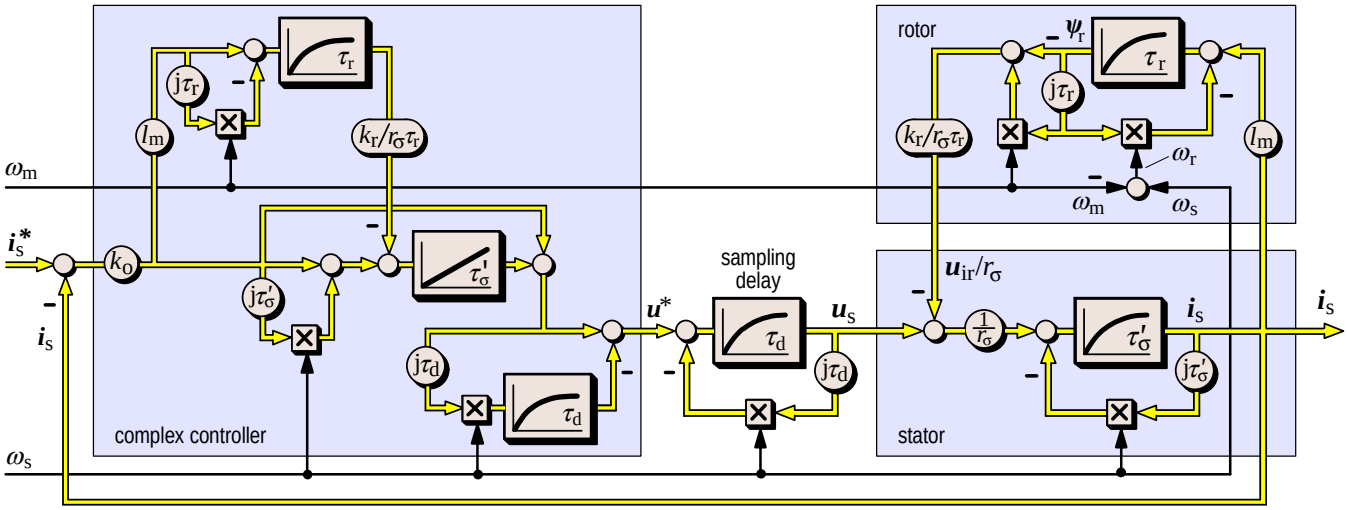

Fig. 16 Current control system using a controller with single-complex poles. The induction motor is represented in the right.

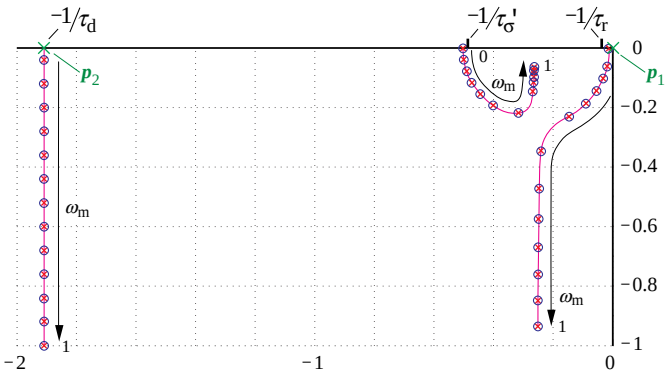

Fig. 17 Roots and poles of the plant and the complex current controller, synchronous coordinates; f_s = 500 Hz, ω_m = 0 … 1 parameter

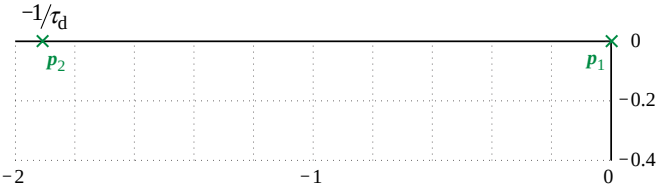

Fig. 18 Roots of the open loop transfer function, complex current controller

$-1/\tau_r - j\omega_s$ as function of ω_s, and an added pole $\boldsymbol{p}_1$ in the origin which serves as an error integrator. The isolated transfer function of this portion is

$$\boldsymbol{F}_{center}(s) = \frac{1 + j\omega_s \tau_\sigma'}{\tau_\sigma' s} + 1 = \frac{\tau_\sigma' s + 1 + j\omega_s \tau_\sigma'}{\tau_\sigma' s} \qquad (16)$$

An additional signal from the upper structure of the complex controller models the rotor, and in combination with (16), the dynamic interaction between the stator and the rotor of the machine. It adds a chain of zeroes $-1/\tau_r - j\omega_m$ as function of ω_m, and a pole at $-1/\tau_r$. In its interaction with (16), it displaces the zeroes of (16) and its own zeroes to be exactly located on the two typical single-complex eigenvalues Fig. 2 of the induction motor. These are then seen eliminated in the right of the root locus plot Fig. 17. The added pole eliminates the zero of (13).

With all single-complex zeroes in the third quadrant of the root locus plane being cancelled, the open loop transfer function resulting from (13), (14) and (15)

$$\boldsymbol{F}_k(s) = k_o \frac{1}{\tau_\sigma' s(\tau_d s + 1)} \qquad (17)$$

has no more complex coefficients; cross-coupling is thus eliminated. The location of the two real roots of (17) is shown in Fig. 18.

The closed loop system is designed for critical damping $D = 1/2\sqrt{2}$ which determines the open loop gain $g_o = \tau'_\sigma / 2\tau_d$.

The step response Fig. 19 obtained from the experimental setup shows the current trajectory moving on the shortest trajectory between the two reference points.

Summary

State-of-the-art current controllers perform unsatisfactorily if applied to PWM controlled voltage source inverters operated at very low switching frequency. The reason is that the dynamics of the drive motor and the inverter are inaccurately modelled. The penalty is a high degree of cross-coupling between the torque-building and the field-generating current component of a vector controlled drive. The common remedy of feedforward compensation of the stator cross-coupling gives little improvement at very low switching frequency.

Modelling the induction motor and the inverter in terms of complex state variables provides a better insight in the dynamics of controlled ac drives. The roots and poles of the respective transfer functions then have the property of being single-complex; the root loci become physically interpretable. It is shown that the sources of cross-coupling are reflected in the unbalanced imaginary parts of three single-complex system roots. The complete elimination of cross-coupling is enabled by a novel type of current controller having three single-complex zeroes. The theory is confirmed by experimental results.

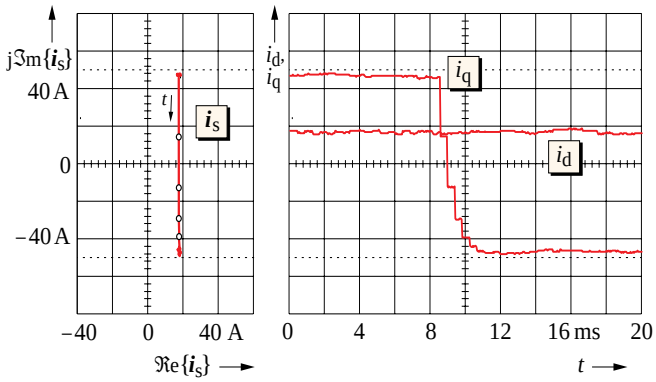

Fig. 19 Recorded step response of the current control system, complex current controller, f_s = 1100 Hz

References

1. P. C. Krause, 0. Wasynczuk, and S. D. Sudhoff, „Analysis of Electric Machinery“, *IEEE Press Book*, New York, 1995.
2. W. Leonhard, „Control of Electrical Drives“, Teubner, Stuttgart 1973.
3. J. Holtz, „The Representation of AC Machine Dynamics by Complex Signal Flow Graphs“, *IEEE Transactions on Industrial Electronics*, Vol. 42, No. 3, 1995, pp. 263-271.
4. J. Holtz, „On the Spatial Propagation of Transient Magnetic Fields in AC Machines“, *IEEE Transactions on Industry Applications*, Vol. 32, No. 4, July/Aug. 1996, pp. 927-937.
5. F. Briz, M. W. Degener and R. D. Lorenz, „Analysis and Design of Current Regulators Using Complex Vectors“, *IEEE Transactions on Industry Applications*, Vol. 32, No.3, May/June 2000, pp. 817-825.
6. P. K. Kovács and E. Rácz, „Transient Phenomena in Electrical Machines“, (in German), *Verlag der Ungarischen Akademie der Wissenschaften*, Budapest, 1959; English edition: *Elsevere Science Publishers*, Amsterdam, 1984.
7. M. P. Kazmierkowski and L. Malesani, „Current Control Techniques for Three-Phase Voltage-Source PWM Converters: A Survey“, *IEEE Transactions on Industrial Electronics*, Vol. 45, No. 5, Oct. 1998, pp. 691-703.
8. J. Holtz, „Pulsewidth Modulation for Electronic Power Converters“, *Proceedings of the IEEE*, Vol. 82, No. 8, Aug. 1994, pp. 1194-1214.
9. F. Britz, M. W. Degener and R. D. Lorenz, „Dynamic Analysis of Current Regulators for AC Motors using Complex Vectors“, *IEEE Transactions on Industry Applications*, Vol. 35, No. 6, Nov/Dez. 1999, pp. 1424-1432.